Breakup of the Fermi Surface Near the Mott Transition in Low-Dimensional Systems

C. Berthod and T. Giamarchi
DPMC, Université de Genève, 24 quai Ernest-Ansermet, 1211 Genève 4, Switzerland

S. Biermann and A. Georges
Centre de Physique Théorique, CNRS-UMR 7644, Ecole Polytechnique, 91128 Palaiseau Cedex, France
(Received 17 February 2006; published 27 September 2006)

We investigate the Mott transition in weakly coupled one-dimensional (1D) fermionic chains. Using a generalization of dynamical mean field theory, we show that the Mott gap is suppressed at some critical hopping $t_\perp^{c2}$. The transition from the 1D insulator to a 2D metal proceeds through an intermediate phase where the Fermi surface is broken into electron and hole pockets. The quasiparticle spectral weight is strongly anisotropic along the Fermi surface, both in the intermediate and metallic phases. We argue that such pockets would look like ''arcs'' in photoemission experiments.

DOI: 10.1103/PhysRevLett.97.136401 PACS numbers: 71.10.Pm, 71.10.Hf, 71.27.+a, 71.30.+h

The formation of a pseudogap phase near the Mott transition in strongly correlated electron systems is a long-standing problem in solid-state physics. Since the observation of a pseudogap in high-T_c superconductors [1], the nature and origin of this phase lies at the core of a heated debate. Several related issues, such as the possible breakup of the Fermi surface (FS) into arcs or pockets [2,3] and the concomitant appearance of ''hot spots'' in the quasiparticle spectrum, have also attracted much attention in recent years. The theoretical description of the Mott transition in two spatial dimensions is particularly difficult [4], however, and a consensus on the nature and properties of the pseudogap has not yet emerged. The central question concerns the way the FS is destroyed when entering the Mott state, either at zero temperature as a function of some control parameter, or with decreasing temperature from a high-T metallic phase.

For solving these questions one has to resort to approximate or numerical approaches. Among those, the Dynamic Mean Field Theory (DMFT) [5,6] has proven to be very fruitful to tackle the question of Mott transitions and strong correlations in high dimensional systems. However, since the standard implementation of this method reduces the problem to a single site, the momentum dependence of the self-energy is lost, which makes it unable to describe FS anisotropies. To overcome this limitation, various cluster-DMFT schemes have been used [7–10]. One difficulty with these approaches which, for small clusters, can affect physical predictions, lies in a certain degree of arbitrariness in converting the cluster results into physical quantities on the lattice.

In addition to high-T_c superconductors, these questions related to the approach of the Mott transition are directly relevant to other systems in which interactions are deemed to be important, such as the organic superconductors, made of weakly coupled one-dimensional chains [11]. Such systems exhibit a deconfinement transition between a one-dimensional Mott insulator and a three-dimensional metal. For such systems, FS pockets were found when the interchain coupling is treated within the RPA approximation [12]. The pockets form when the interchain bandwidth exceeds the 1D Mott gap of the chains. However the RPA approximation neglects the feedback of the interchain hopping on the 1D Mott gap, and more generally on the self-energy. To go beyond this approximation it is useful to generalize the one-site DMFT to one-dimensional chains embedded in a self-consistent bath [13,14]. This ch-DMFT scheme was successfully applied to study the deconfinement transition in quasi-1D lattices, and is the ideal tool to investigate the Mott transition in this type of systems [15–17].

In the present Letter, we use this method to study a 2D lattice of spinless fermions made of weakly coupled 1D chains. Contrarily to the 1D Hubbard model, the 1D spinless model has a Mott transition for a finite value of the interaction. Furthermore, the effects of the interaction are stronger in the spinless case than in the spin-$\frac{1}{2}$ case, as illustrated by the lower value of the Luttinger coefficient which can be reached in the former. The spinless model can also be viewed as a caricature of a spin-$\frac{1}{2}$ model at quarter filling with a very strong local repulsion. Using the ch-DMFT method we show that FS pockets exist in this model close to the metal-insulator transition. However, due to the very strong anisotropy of the spectral weight along the Fermi surface, these pockets would appear as Fermi arcs in experiments. We note that similar effects have been recently discussed using extensions of DMFT including momentum dependence [18,19].

Our model has two parameters, $t_\perp$ and V, which control the interchain hopping and the interaction $\mathcal{H}_{\text{int}} = V\sum_r n_r n_{r+1}$ within the chains, respectively, relative to the in-chain hopping t. In the 1D limit ($t_\perp = 0$) this model has a phase transition from a Luttinger liquid at $V < 2t$ to a Mott insulator at $V > 2t$. Here we focus on the region $V > 2t$, and we investigate the destruction of the Mott insulator with increasing $t_\perp$. Within ch-DMFT the 2D problem is

mapped onto an effective 1D problem described by the action $\mathcal{S}_{\rm eff} = \mathcal{S}^0_{\rm eff} + \int_0^\beta d\tau \mathcal{H}_{\rm int}$ with

$$\mathcal{S}^0_{\rm eff} = -\sum_{rr'} \int_0^\beta d\tau d\tau' c_r^\dagger(\tau) \mathcal{G}_0^{-1}(r - r', \tau - \tau') c_{r'}(\tau'). \quad (1)$$

The inverse propagator $\mathcal{G}_0^{-1}$ in Eq. (1) plays the role of a long-range, time-dependent hopping amplitude. It must be determined from the requirement that the in-chain Green's function $\mathcal{G}$ calculated from $\mathcal{S}_{\rm eff}$ coincides with the $k_\perp$-summed Green's function of the original 2D model, $G(\boldsymbol{k}, \omega) = [\omega - \xi_k - \varepsilon_\perp - \Sigma(k, \omega)]^{-1}$ [5,15]. This requirement implies

$$\mathcal{G}_0^{-1}(k, \omega) = \omega - \xi_k + \mathcal{G}^{-1}(k, \omega) - R[\mathcal{G}(k, \omega)], \quad (2)$$

with k the in-chain momentum, $\xi_k = -2t\cos k - \mu$ the bare dispersion, and $R(z) = \text{sign}[\text{Re}(z)]\sqrt{1/z^2 + (2t_\perp)^2}$ resulting from the integration over the transverse energy $\varepsilon_\perp = -2t_\perp \cos(k_\perp)$. Equations (1) and (2) can be readily derived from the assumption that the lattice self-energy does not depend on transverse momentum $k_\perp$, and is given by the effective in-chain self-energy:

$$\Sigma(k, \omega) = \mathcal{G}_0^{-1}(k, \omega) - \mathcal{G}^{-1}(k, \omega). \quad (3)$$

$\Sigma(k, \omega)$ will be our main concern here. In order to evaluate the self-energy we compute the space-time Green's function $\mathcal{G}(r, \tau) = -\langle c_r(\tau) c_0^\dagger(0)\rangle$ by quantum Monte Carlo (QMC) calculations on a discrete imaginary-time mesh $\tau_\ell = \ell\beta/L$, using the Hirsch-Fye algorithm [20]. From the Fourier transform $\mathcal{G}(k, i\omega_n)$ we construct a new propagator $\mathcal{G}_0$ according to Eq. (2), which is fed back into Eq. (1) until self-consistency is achieved.

We consider a half-filled 32-site chain closed with antiperiodic boundary conditions (BC). These BC were adopted for two reasons: (i) in short 1D chains we observed that the convergence of the QMC calculations toward exact-diagonalization results is much faster with antiperiodic than with periodic BC; (ii) for a given system size, the antiperiodic BC improve the resolution near $k = \pi/2$, which is an advantage for the investigation of the FS properties. The shape of the FS is indeed controlled by the real part of the self-energy through the equation

$$\xi_k - 2t_\perp \cos(k_\perp) = -\text{Re}\Sigma(k, i0^+), \quad (4)$$

which must be solved at zero temperature near $k = \pi/2$. At finite temperature the FS looses its identity, although sharp signatures may subsist in the zero-energy spectral function $A(\boldsymbol{k}, \omega = 0)$, which is accessible through photoemission experiments. We will first discuss the FS topology and properties implied by Eq. (4) and our ch-DMFT results for $\Sigma(k, \omega)$, before addressing some issues related to the experimental measurement of the FS.

For evaluating Eq. (4) one needs a procedure to continue the ch-DMFT self-energy from the lowest Matsubara frequency $i\omega_0 = i\pi T$ down to $\omega = i0^+$ along the imaginary-frequency axis. This is a delicate endeavor, which in general requires some assumption about the analytical behavior of $\Sigma(k, \omega)$ near $\omega = 0$. We performed the continuation by fitting the self-energy to an analytical function. The prominent feature in the Mott phase is the spectral gap which can be crudely represented by a self-energy $\Sigma_\Delta(k, \omega) = (\lambda - 1)\xi_k + (\Delta/2)^2/(\omega + \lambda\xi_k)$, where Δ is the gap and λ accounts for the dispersion renormalization due to exchange. A similar Ansatz was recently proposed to describe high-T_c superconductors [21]. This simple form is not sufficient to reproduce our QMC results, however, even in the pure Mott phase at $t_\perp = 0$. We obtained a much better agreement with our data by taking into account residual interactions. Specifically, the self-energy to which we fit the QMC results is $\Sigma(k, \omega) = \Sigma_\Delta(k, \omega) + \Sigma_{\rm int}(k, \omega)$, where $\Sigma_{\rm int}$ contains all diagrams—evaluated using the *gapped* propagator $G_0(k, \omega) = [\omega - \xi_k - \Sigma_\Delta(k, \omega)]^{-1}$ and an effective interaction V^*—up to second order in perturbation theory. A comparison of the QMC data and model self-energies is displayed in Fig. 1. One can see that the model has enough freedom to fit the QMC results in great detail, especially in the low-frequency region we are mostly interested in. It turns out that the model fits the QMC data in the whole range of temperature and $t_\perp$ values which we have investigated. We can therefore use this fit to track the closing of the Mott gap and the formation of the Fermi surface as $t_\perp$ is increased. A few additional illustrations of the fit performance can be seen in Fig. 2.

In Fig. 2 we display our results for $-\text{Re}\Sigma(k, i\omega_0)$ at $V = 2.5t$ and different values of $t_\perp$, together with the fit results evaluated at $i\omega_0$ and $i0^+$. The main trend with increasing $t_\perp$ can be seen on the raw numerical data. For small $t_\perp$ the self-energy has a tendency to diverge near $k_F = \pi/2$

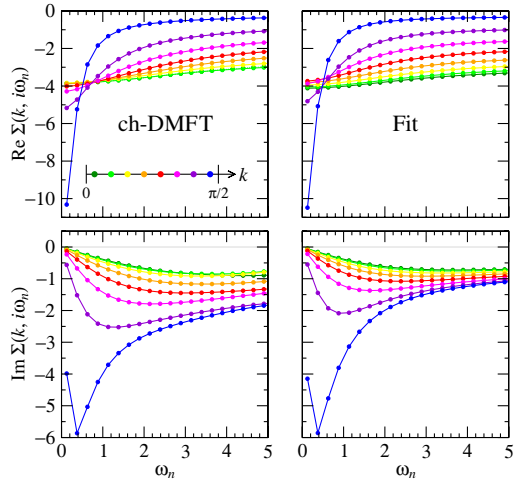

FIG. 1 (color online). Left panels: Self-energy on the imaginary-frequency axis for k between 0 and $\pi/2$ at $V = 4$, $t_\perp = 0.5$, and $T = 0.04$. The dots show the numerical data and the lines are guides to the eye. The number of imaginary-time slices was $L = 60$. Right panels: Fit of the numerical data to a trial self-energy (see text). All energies are in units of t.

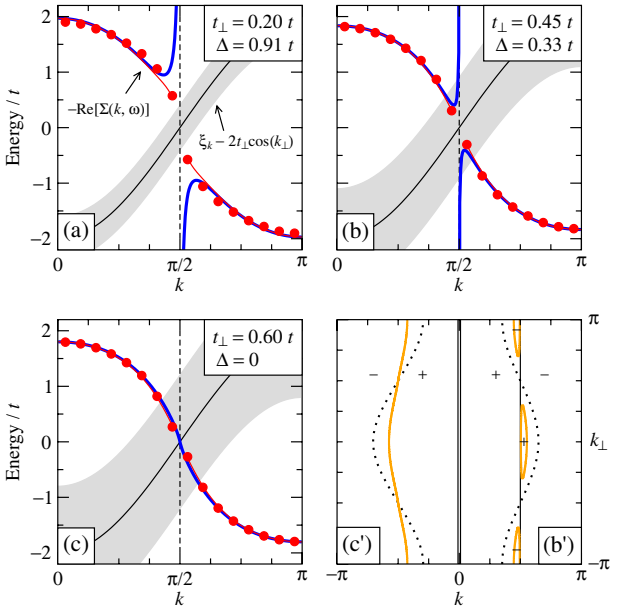

FIG. 2 (color online). (a)–(c) Real part of the ch-DMFT self-energy as a function of k at the lowest Matsubara frequency for $V = 2.5$, $T = 0.1$, and increasing $t_\perp$ (red points). The red and blue lines show the fit of the data to the function $\Sigma_\Delta + \Sigma_{\rm int}$ at $\omega = i\omega_0$, $T = 0.1$, and at $\omega = i0^+$, $T = 0$, respectively. The shaded areas show the domain covered by the free dispersion $\xi_k - 2t_\perp\cos(k_\perp)$ in Eq. (4). The Fermi surfaces corresponding to (b) and (c) are shown in (b′) and (c′). The dotted lines indicate the noninteracting Fermi surfaces, and the + and − show the sign of $\mathrm{Re}G(\boldsymbol{k}, 0)$.

[Fig. 2(a)]. This behavior is most clearly seen at large V and low T (see Fig. 1). The singularity of $\mathrm{Re}\Sigma(k, 0)$ results from the presence of a gap in the zero-temperature spectral function at k_F [22], and is well captured by the model self-energy evaluated at $T = 0$ (blue line) [23]. At finite frequency and/or temperature the singularity is regularized as shown by the red line. With increasing $t_\perp$ the drop of the QMC self-energy across k_F diminishes [Fig. 2(b)]. Correspondingly, the fitted spectral gap Δ decreases and eventually vanishes at $t_\perp^{c2} \sim 0.5t$, together with the disappearance of the singularity in the self-energy [Fig. 2(c)].

Figure 2 provides the graphical solution of Eq. (4), and illustrates the formation of the Fermi-surface pockets in this model. When $t_\perp$ is small, the transverse dispersion is not sufficient to overcome the gap in the self-energy, and the system remains insulating. At high $t_\perp$, on the contrary, there is no gap in the self-energy and Eq. (4) has a solution for all $k_\perp$, leading to a continuous Fermi surface. The latter has practically the same shape as the noninteracting FS, but is strongly renormalized to an effective interchain hopping $t_\perp^* \approx 0.41t_\perp$. In the intermediate regime $t_\perp^{c1} < t_\perp < t_\perp^{c2}$, there is a finite range of $k_\perp$ values where Eq. (4) admits two solutions, leading to the breakup of the FS into pockets [Fig. 2(b) and 2(b′)].

According to Luttinger's theorem, the area of the Brillouin zone where $\mathrm{Re}G(\boldsymbol{k}, 0) > 0$ equals the electron density and is thus conserved [12,24]. In the Mott phase $\mathrm{Re}G(\boldsymbol{k}, 0)$ changes sign at $k = \pm\pi/2$ due to the divergence of $\Sigma(k, 0)$ [Fig. 2(a)], and is positive in the domain $|k| < \pi/2$, leading to a density $n = 1/2$ as expected. Because the singularity of $\Sigma(\pm\pi/2, 0)$ subsists as long as $\Delta > 0$, the line of zeros of $\mathrm{Re}G(\boldsymbol{k}, 0)$ at $k = \pm\pi/2$ is still present when FS pockets develop, as indicated in Fig. 2(b′). On the other hand, owing to particle-hole symmetry the electron and hole pockets have identical volumes, so that Luttinger theorem is obeyed in our results.

The mechanisms of FS pockets formation in the present study and in the RPA approach of Ref. [12] are similar, although there is one important difference. In RPA the spectral gap keeps its 1D value at all $t_\perp$: pockets form when $t_\perp > t_\perp^{c1} \sim \Delta_{\rm 1D}$, and they never merge into a connected Fermi surface as $t_\perp$ continues increasing. Within ch-DMFT, in contrast, the closing of the Mott gap with increasing $t_\perp$ is correctly captured; as a result the pockets form at lower $t_\perp$ values—thus they are very thin—and eventually they disappear at $t_\perp^{c2}$ where $\Delta = 0$.

The quasiparticle properties are strongly anisotropic along the FS pockets. It is already clear from Fig. 2(b) that the spectral weight is much smaller on the vertical parts of the pockets closest to $k = \pi/2$, due to the diverging self-energy in this region; as a result the pockets would most likely look like "arcs" in photoemission experiments (see below). Figure 3(a) shows the evolution of the quasiparticle residue along the Fermi surface. The residue was evaluated as $Z = [1 - d\,\mathrm{Re}\Sigma(k, \omega)/d\omega|_{\omega=0}]^{-1}$, using the model self-energy and an interpolation of the parameters fitted to the ch-DMFT data in the whole range of $t_\perp$ values [Fig. 3(b)]. In the intermediate phase the residue on the vertical segments of the pockets decreases from $Z \sim 0.15$ to $Z \sim 0$ with increasing $t_\perp$. On the "cold" side of the pockets the behavior is inverted, and the residue increases from $Z \sim 0.35$ to $Z \sim 0.5$. Strikingly, a hot spot around $\boldsymbol{k} = (\pi/2, \pi/2)$ subsists at $t_\perp > t_\perp^{c2}$. Here again the evolution of Z with $t_\perp$ is different at the cold and hot spots: while Z steadily approaches 1 in the cold region, it remains close to $Z \sim 0.4$ at the hot spots.

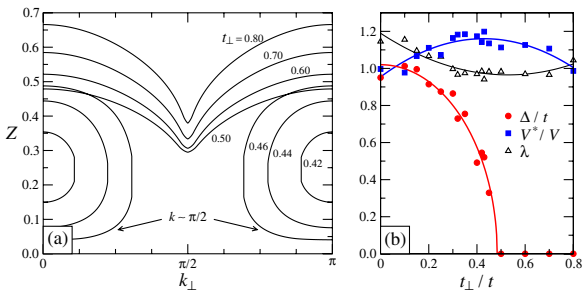

FIG. 3 (color online). (a) Evolution of the quasiparticle residue Z along the Fermi surface for different interchain couplings $t_\perp$. When FS pockets are present there are two values of Z for each $k_\perp$, the lowest value corresponding to the region of the pocket closest to $k = \pi/2$. (b) Parameters of the model self-energy determined from fits to the ch-DMFT numerical data.

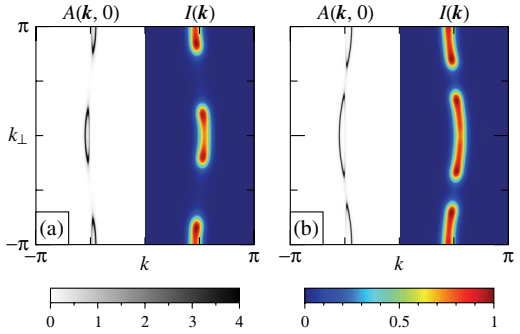

FIG. 4 (color online). Comparison of the zero-energy spectral function $A(\boldsymbol{k}, 0)$ at $T = 0$ with the expected ARPES intensity $I(\boldsymbol{k})$ calculated assuming a k-space resolution of 0.04π, an energy resolution $0.004t$, and an energy integration window $\delta E = 0.01t$. The self-energy parameters are taken from Fig. 3(b) for $t_\perp = 0.42$ (a) and $t_\perp = 0.46$ (b).

It is worth stressing the role of residual interactions in the results of Figs. 2 and 3(a). At the qualitative level, the self-energy $\Sigma_\Delta(k, \omega)$ (with $\lambda = 1$) is sufficient to understand the formation of FS pockets with anisotropic residues. Using $\Sigma = \Sigma_\Delta$ in Eq. (4) one indeed finds that pockets form for $0 < \Delta < 2t_\perp$, and that the residue varies on such pockets. However the pockets obtained in this way are considerably wider than in Fig. 2, and the residue in the cold regions is $Z \sim 1$ when Δ approaches zero instead of $Z \sim 0.5$ as in Fig. 3. Thus the residual interactions are important for the quantitative understanding of the FS properties. Meanwhile, the fact that our model self-energy fits the ch-DMFT data at $t_\perp > t_\perp^{c2}$ with $V^* \sim V$ [Fig. 3(b)] indicates that second-order perturbation theory is a good approximation in this region, as expected in a Fermi liquid.

We now turn to the question of the experimental observation of FS pockets. There are several limitations which could make the observation of such pockets by angle-resolved photoemission spectroscopy (ARPES) challenging, such as the finite energy and momentum resolutions, the finite temperature at which experiments are performed, as well as the need to integrate the ARPES intensity on some energy window in order to improve the signal to noise ratio. Ideally, ARPES would measure the occupied spectrum $A(\boldsymbol{k}, \omega) f(\omega)$. In practice, however, due to the above limitations, the measured intensity at the Fermi energy would be $I(\boldsymbol{k}) \propto \int_{-\delta E}^{\infty} d\omega \int d\varepsilon d\boldsymbol{q} A(\boldsymbol{q}, \varepsilon) f(\varepsilon) g(\boldsymbol{k} - \boldsymbol{q}, \omega - \varepsilon)$, where δE defines the energy integration window and g is some function describing the instrument resolution. We have calculated $I(\boldsymbol{k})$ using a Gaussian for g. The comparison depicted in Fig. 4 of the $T = 0$ Fermi surface with the expected ARPES intensity clearly shows that the closing segments of the pockets near $k = \pi/2$ would very likely be hidden in the ARPES signal. The broad aspect of $I(\boldsymbol{k})$ as compared to $A(\boldsymbol{k}, 0)$ is not a consequence of finite temperature, but of (i) the finite k-space resolution combined with the fact that the pockets are very thin and (ii) the large difference in quasiparticle weight on the two sides of the pockets, which is obvious in $A(\boldsymbol{k}, 0)$ and consistent with the residues shown in Fig. 3. Similar FS anisotropies were recently found in cluster-DMFT studies of the 2D Hubbard model [18], suggesting that such effects are generic to systems close to a Mott transition, and could possibly explain the ARPES observation of FS arcs in high-T_c cuprate superconductors.

We are grateful to G. Kotliar for useful discussions and to F. C. Zhang and P. W. Phillips for letting us know about their work [21,22] as this Letter was being written. This work was supported by the Swiss National Science Foundation through Division II and the NCCR program MaNEP, as well as by CNRS and Ecole Polytechnique.

[1] T. Timusk and B. Statt, Rep. Prog. Phys. **62**, 61 (1999).
[2] M. R. Norman *et al.*, Nature (London) **392**, 157 (1998).
[3] A. Damascelli, Z. Hussain, and Z.-X. Shen, Rev. Mod. Phys. **75**, 473 (2003).
[4] M. Imada, A. Fujimori, and Y. Tokura, Rev. Mod. Phys. **70**, 1039 (1998).
[5] A. Georges, G. Kotliar, W. Krauth, and M. J. Rozenberg, Rev. Mod. Phys. **68**, 13 (1996).
[6] G. Kotliar and D. Vollhardt, Phys. Today **57**, No. 3, 53 (2004).
[7] T. Maier, M. Jarrell, T. Pruschke, and M. H. Hettler, Rev. Mod. Phys. **77**, 1027 (2005).
[8] A.-M. S. Tremblay, B. Kyung, and D. Sénéchal, Fiz. Nizk. Temp. **32**, 561 (2006).
[9] G. Kotliar *et al.*, Rev. Mod. Phys. **78**, 865 (2006).
[10] O. Parcollet, G. Biroli, and G. Kotliar, Phys. Rev. Lett. **92**, 226402 (2004).
[11] T. Giamarchi, Chem. Rev. **104**, 5037 (2004).
[12] F. H. L. Essler and A. M. Tsvelik, Phys. Rev. B **65**, 115117 (2002).
[13] E. Arrigoni, Phys. Rev. Lett. **83**, 128 (1999).
[14] A. Georges, T. Giamarchi, and N. Sandler, Phys. Rev. B **61**, 16 393 (2000).
[15] S. Biermann, A. Georges, A. Lichtenstein, and T. Giamarchi, Phys. Rev. Lett. **87**, 276405 (2001).
[16] S. Biermann, A. Georges, T. Giamarchi, and A. Lichtenstein, in *Strongly Correlated Fermions and Bosons in Low Dimensional Disordered Systems*, edited by I. V. Lerner *et al.* (Kluwer, Dordrecht, 2002), p. 81.
[17] T. Giamarchi, S. Biermann, A. Georges, and A. Lichtenstein, J. Phys. IV **114**, 23 (2004).
[18] T. D. Stanescu and G. Kotliar, cond-mat/0508302.
[19] E. Z. Kuchinskii, I. A. Nekrasov, and M. V. Sadovskii, Low Temp. Phys. **32**, 398 (2006).
[20] J. E. Hirsch and R. M. Fye, Phys. Rev. Lett. **56**, 2521 (1986).
[21] K.-Y. Yang, T. M. Rice, and F.-C. Zhang, Phys. Rev. B **73**, 174501 (2006).
[22] T. D. Stanescu, P. W. Phillips, and T.-P. Choy, cond-mat/0602280.
[23] A gap in the self-energy could also result from the presence of charge order in the system. In our QMC data, however, the inhomogeneity of the charge density is less than 1%, which is way too small to explain the large gaps seen in Fig. 3.
[24] I. Dzyaloshinskii, Phys. Rev. B **68**, 085113 (2003).